

The photon parton distribution function: updates and applications

Aneesh Manohar, Paolo Nason, Gavin Salam, and Giulia Zanderighi¹

Abstract

The photon parton distribution function (PDF) of the proton is crucial for precise comparisons of LHC cross sections with theoretical predictions. However, it was previously affected by very large uncertainties of around $\mathcal{O}(100\%)$ or dependent upon phenomenologically inspired models. In the paper [1], we demonstrated how the photon PDF could be determined using the proton structure functions F_2 and F_L measured in electron–proton scattering experiments. We provided an explicit formula for the PDF, which can be systematically improved order by order in perturbation theory. We obtained a photon PDF with errors $\lesssim 2\%$ for $10^{-4} < x < 0.1$. Here, we recall the underlying idea and method used to obtain this result, as well as the progress made since then.

1 Introduction

Hard scattering processes involving hadrons can be computed in terms of parton distribution functions (PDFs) $f_{a/H}(x, \mu^2)$, which represent the probability of finding a parton a with momentum fraction x in a hadron target H .² These distributions depend logarithmically on the renormalisation and factorisation scale μ due to radiative corrections. This principle underlies most studies conducted at CERN’s Large Hadron Collider (LHC). Of course, the primary partons are quarks and gluons.

It has been known for a long time that ultra-relativistic charged particles generate an electromagnetic field that can be interpreted as a distribution of photons, as originally calculated by Fermi, Weizsäcker and Williams [2–4] for point-like particles. The same principle applies to the proton and its constituents. Due to the weakness of the electromagnetic coupling, the photon density in the proton had long been considered of secondary importance. However, between 2010 and 2016, it was realised that knowledge of the photon PDF was becoming more important as the measurements at the LHC became increasingly precise. The uncertainty on the photon PDF was limiting our ability to predict certain key reactions at the LHC. Notable examples include the production of the Higgs boson through

¹Speaker at the 2024 International Conference of Basic Science, presenting the paper [1], which received the 2024 Frontier of Science Award in Theoretical Physics.

²From now on, we will only discuss proton targets, and omit the subscript H .

W/Z fusion [5] or in association with an outgoing weak boson [6]. For $W^\pm H$ production, it was the largest source of uncertainty [7]. The photon distribution was also relevant for the production of lepton pairs [8–12], top quarks [13], pairs of weak bosons [14–20] and generally for electroweak corrections in almost any LHC process. At that time, the available results on the photon PDF, such as MRST2004qed [21], NNPDF23_qed [22] CT14qed_inc [23] and the HKR16 set [24], either had large uncertainties, or relied upon phenomenologically inspired models.

In 2015, the lack of a precise knowledge of the photon PDF became an even more concerning issue with the observation of a 750 GeV resonance in $\gamma\gamma$ final states by the ATLAS [25] and CMS [26] experiments.³ This observation, which generated much excitement in the high-energy physics community, suggested that the resonance could have been produced in $\gamma\gamma$ annihilation, highlighting the need for a sound knowledge of the photon PDF.

In [1, 27] we derived a formula for the photon PDF given in terms of the electromagnetic form factors and structure functions of the proton, which are very accurately measured. The main idea leading to this work was that in a reaction involving a virtual, spacelike photon, one cannot really distinguish whether the photon is incoming or outgoing. Hence, it should be possible to express the photon PDF, typically associated with photon emission from the proton, in terms of the proton structure function, associated with photon absorption by the proton. In fact, in the frame where the proton is at rest, the proton absorbs the spacelike photon emitted by the electron, while in the centre-of-mass frame of the lepton, the opposite occurs.

To compute the photon PDF, we considered a simple photon-initiated processes, and computed it in two different ways: in terms of an (unknown) photon PDF, and in terms of the lepton-hadron scattering hadronic tensor and form factors. Equating the two results allowed us to extract the unknown photon PDF in terms of electron-proton scattering data.⁴ The precision of our result for the photon PDF was thus a consequence of the precision of the available lepton-proton scattering data. We stress that this data is needed even at relatively low energies, i.e. the structure functions in the deep-inelastic (DIS) limit are not sufficient for our purposes. However, the required data was available, having been accumulated over many years of nuclear physics experiments.

In [1] we carried out the calculation using the production of a hypothetical heavy lepton in electron-proton collisions, mediated by a flavour violating magnetic moment interaction, as a hard probe. We provided a formula for the photon PDF of the proton $f_\gamma(x, \mu^2)$ as an integral over proton structure functions $F_2(x, Q^2)$ and $F_L(x, Q^2)$, including all terms of order $\mathcal{O}(\alpha)$ and with errors of order $\mathcal{O}(\alpha^2 L)$ and $\mathcal{O}(\alpha\alpha_s)$, where L is the logarithm of μ divided by a typical hadronic scale.⁵ This

³The resonance disappeared in 2016 when new data became available.

⁴This crucial observation in Ref. [1] was partly inspired by Drees and Zeppenfeld’s study of supersymmetric particle production at ep colliders [28]. Our perspective was also implicit in Refs. [29, 30].

⁵The photon PDF $f_\gamma(x, \mu^2)$ is of order αL . The result in Ref. [1] included terms of order $\alpha^2 L^2 (\alpha_s L)^n$ and $\alpha (\alpha_s L)^n$, but not of order $\alpha^2 L$. By assuming $L \approx 1/\alpha_s$, and considering that $\alpha_s^2 \approx \alpha$, we see that the first subleading terms to include are of order α (i.e. one power of L less than the leading term) and of order $\alpha^2 L^2$.

formula enabled us to obtain the photon PDF with an uncertainty of less than 3% over a wide range of x values, $10^{-5} \leq x \leq 0.5$. This reduced the uncertainty by a factor of about forty compared to previous photon PDF determinations, such as MRST2004qed [21] and NNPDF23_qed [22], which relied on fits to LHC data and/or modelling.

The derivation in [1] was extended in [27], where we re-derived our formula for the photon PDF using as a hard probe a hypothetical scalar produced via $\gamma\gamma$ annihilation in proton-photon collisions, thus checking the universality of our result. Furthermore, we provided another independent derivation by defining the photon PDF as the light-cone Fourier transform of the two-point function of electromagnetic field-strength tensors. This approach gives a representation for the photon PDF that is *exact*, i.e. valid to all orders in the strong and electromagnetic interactions, and that can in principle be used to compute the photon PDF at arbitrarily high orders in perturbation theory. It was used to obtain expressions for the photon PDF including all terms of order $\alpha\alpha_s$ and α^2 , one order higher in $\alpha_s(\mu)$ or $\alpha(\mu)$ than the result in [1]. Furthermore, results were also given for polarised photons and transverse-momentum dependent PDFs.

2 Definitions and notation

We define the physical electromagnetic e_{ph} in terms of the vacuum polarisation function $\Pi(q^2, \mu^2)$,

$$e_{\text{ph}}^2(q^2) = \frac{e^2(\mu^2)}{1 - \Pi(q^2, \mu^2)}, \quad (2.1)$$

which depends on q^2 , but is independent of μ^2 . Thus $\alpha_{\text{ph}}(0) = e_{\text{ph}}^2(0)/4\pi$ is the usual fine structure constant $\simeq 1/137.036$ measured in atomic physics. Eq. (2.1) is used in the spacelike region $q^2 < 0$, where $\Pi(q^2, \mu^2)$ is real.

The proton hadronic tensor, which enters the cross section formula for deep-inelastic scattering, is defined as

$$W_{\mu\nu}(p, q, s) = \frac{1}{4\pi} \int d^4z e^{iq \cdot z} \langle p, s | [j_\mu(z), j_\nu(0)] | p, s \rangle, \quad (2.2)$$

where j_μ is the electromagnetic current, p is the incoming proton momentum, q is the photon momentum (transferred to the proton) and s denotes the proton spin. The conventional decomposition of $W_{\mu\nu}$ into structure functions is

$$\begin{aligned} W_{\mu\nu}(p, q, s) = & F_1 \left(-g_{\mu\nu} + \frac{q_\mu q_\nu}{q^2} \right) + \frac{F_2}{p \cdot q} \left(p_\mu - \frac{p \cdot q}{q^2} q_\mu \right) \left(p_\nu - \frac{p \cdot q}{q^2} q_\nu \right) \\ & + \frac{ig_1}{p \cdot q} \epsilon_{\mu\nu\lambda\sigma} q^\lambda s^\sigma + \frac{ig_2}{(p \cdot q)^2} \epsilon_{\mu\nu\lambda\sigma} q^\lambda (p \cdot q s^\sigma - s \cdot q p^\sigma). \end{aligned} \quad (2.3)$$

The proton spin four-vector s is normalised so that $p \cdot s = 0$, $s \cdot s = -m_p^2$, where m_p is the proton mass. The structure functions F_1 , F_2 , g_1 and g_2 are functions of

$$x_{\text{bj}} = \frac{Q^2}{2p \cdot q} \quad (2.4)$$

and Q^2 . We also introduce the longitudinal structure function

$$F_L(x_{\text{bj}}, Q^2) \equiv \left(1 + \frac{4x_{\text{bj}}^2 m_p^2}{Q^2}\right) F_2(x_{\text{bj}}, Q^2) - 2x_{\text{bj}} F_1(x_{\text{bj}}, Q^2), \quad (2.5)$$

and write our results using F_2 and F_L instead of F_2 and F_1 .

3 Photon PDF Formula

The formula for the photon PDF was obtained by using as a hard probe a toy-process, the scattering of a heavy neutral lepton off a proton via a magnetic moment interaction. We verified the result by carrying out the same derivation using as a probe the production of a scalar particle via photon-photon fusion and also by using the definition of PDF operators in terms of light-cone Fourier transforms in [27].

It is convenient to split the photon PDF into two pieces,

$$f_\gamma(x, \mu^2) = f_\gamma^{\text{PF}}(x, \mu^2) + f_\gamma^{\text{con}}(x, \mu^2), \quad (3.1)$$

referred to as the ‘‘physical factorisation’’ and ‘‘ $\overline{\text{MS}}$ -conversion’’ terms. The $\overline{\text{MS}}$ -conversion is an additional finite contribution to the photon PDF obtained by applying the $\overline{\text{MS}}$ subtraction scheme to regulate UV divergences in the factorization formula order-by-order in perturbation theory.

The physical factorization term is exact,

$$f_\gamma^{\text{PF}}(x, \mu^2) = \frac{1}{2\pi\alpha(\mu^2)x} \int_x^1 \frac{dz}{z} \int_{\frac{m_p^2 x^2}{1-z}}^{\frac{\mu^2}{1-z}} \frac{dQ^2}{Q^2} \alpha_{\text{ph}}^2(-Q^2) \left\{ -z^2 F_L(x/z, Q^2) + \left[2 - 2z + z^2 + \frac{2m_p^2 x^2}{Q^2} \right] F_2(x/z, Q^2) \right\}. \quad (3.2)$$

The $\overline{\text{MS}}$ -conversion term has the perturbative expansion

$$f_\gamma^{\text{con}}(x, \mu^2) = \sum_{r \geq 0, s \geq 1} \left(\frac{\alpha_s}{2\pi}\right)^r \left(\frac{\alpha}{2\pi}\right)^s f_\gamma^{(r,s)}(x, \mu^2), \quad (3.3)$$

where the couplings are evaluated at μ^2 . At leading order the $\overline{\text{MS}}$ -conversion term is [1]

$$f_\gamma^{(0,1)}(x, \mu^2) = \frac{1}{x} \int_x^1 \frac{dz}{z} (-z^2) F_2(x/z, \mu^2) + \mathcal{O}(\alpha^2, \alpha\alpha_s). \quad (3.4)$$

The next order contributions $f_\gamma^{(1,1)}$ and $f_\gamma^{(0,2)}$ are given in [27].

4 Experimental Inputs

To evaluate the photon parton density we require information on the F_2 and F_L structure functions over the full x, Q^2 allowed kinematic range. Using $L \sim \ln \mu^2/m_p^2$, we include terms $\alpha L(\alpha_s L)^n$ at lowest order and $\alpha(\alpha_s L)^n, \alpha^2 L^2(\alpha_s L)^n$ corrections at higher order. The physical factorization term is enhanced by L relative to the $\overline{\text{MS}}$ -conversion term due to the additional integral over Q^2 in Eq. (3.2).

The F_2 and F_L structure functions are most commonly determined from electron–proton scattering data. We separate the data inputs according to the kinematic region and the corresponding final state in ep scattering. The main kinematic variables for the separation will be Q^2 and W^2 where

$$W^2 = m_p^2 + \frac{1 - x_{\text{bj}}}{x_{\text{bj}}} Q^2, \quad (4.1)$$

is the squared invariant mass of the outgoing system associated with the hadronic side of the collision.

Elastic contribution: In our definition, the elastic contribution corresponds to the region of $W < m_p + m_{\pi^0}$. In particular it includes configurations where one or more photons are radiated from the proton.⁶ Experimental data on elastic scattering is usually corrected for radiation from the proton, since the measurements are performed with the goal of extracting the electric and magnetic Sachs form factors of the proton, G_E and G_M respectively. A widely used approximation for the $G_{E,M}$ form factors is the dipole form,

$$G_E^{\text{dip}}(Q^2) = \frac{1}{(1 + Q^2/m_{\text{dip}}^2)^2}, \quad G_M^{\text{dip}}(Q^2) = \mu_p G_E(Q^2), \quad (4.2)$$

where $m_{\text{dip}}^2 = 0.71 \text{ GeV}^2$ and $\mu_p \simeq 2.793$ is the anomalous magnetic moment of the proton. For $Q^2 = 0$ this form yields the exact results $G_E(0) = 1$ and $G_M(0) = \mu_p$, while elsewhere it is an approximation.

For accurate results, the dipole approximation, Eq. (4.2), is not sufficient. The most recent extensive experimental study of the form factors comes from the A1 collaboration [31]. The A1 data itself is limited to $Q^2 \lesssim 1 \text{ GeV}^2$, however the work includes fits to global data up to $Q^2 \sim 10 \text{ GeV}^2$. The electric and magnetic form factor fits are shown in Fig. 1, normalised to the dipole form. Both fits show clear deviations from the dipole form. Note that the fits extend only up to $Q^2 = 10 \text{ GeV}^2$ and beyond this point we use the dipole shape, normalised to the fitted $G_{E/M}(Q^2)$ at $Q^2 = 10 \text{ GeV}^2$. We treat the fit uncertainties on the elastic and magnetic components as 100% correlated, which is the most conservative assumption.

⁶For the determination of the structure functions we find it useful to think of a process in which there can be at most one exchanged photon between the probe and the proton, as in the process of Sec. 3. In actual electron-proton scattering experiments there can be two or more exchanged photons, either real or virtual. These corrections are beyond our accuracy and cannot be classified in terms of the usual electromagnetic structure functions, since they correspond to a more complex tensor structure.

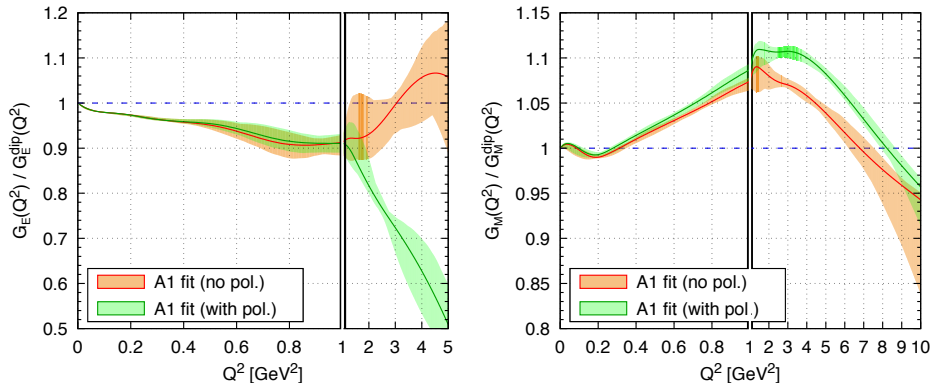


Figure 1: Elastic form factors (ratio to standard dipole form) for the electric (left) and magnetic (right) as fitted by the A1 collaboration [31] with and without polarised data. Note the change in scale at $Q^2 = 1 \text{ GeV}^2$ along the x axis.

Low- Q^2 region: In addition to the elastic component, we need the inelastic part. This corresponds to the region of $W > m_p + m_{\pi^0}$. We split the inelastic part into several sub-regions. At low Q^2 , the structure functions cannot be computed from parton distribution functions and we must rely on direct measurements and theoretical model-independent constraints.

There is a wealth of data covering the low Q^2 region. Rather than using these data directly, we will rely on existing fits of those data. Fits generally focus upon either the resonance region, $W^2 \lesssim 3 \text{ GeV}^2$ or the continuum region, $W^2 \gtrsim 4 \text{ GeV}^2$. Fig. 2 (left) shows data from the CLAS experiment [32], compared to two global fits to resonance region data. The figure (which includes only a small subset of the available data) illustrates the coverage in Q^2 and the quality of the available data. The data is shown as a function of W^2 in order to clearly show the resonance peaks starting with the Δ resonance and beyond. The CLAS fit is intended for use only for $Q^2 > 0.5 \text{ GeV}^2$, while the Christy-Bosted [33] fit is intended for use down to $Q^2 = 0$ and explicitly includes photoproduction data. Comparing the CLAS and Christy-Bosted fits at Q^2 values below the quoted validity range of the CLAS fit shows, however, that they are relatively similar.

For the continuum region, the HERMES collaboration has provided a fit, GD11-P [34], using a wide range of data and the ALLM [35] functional form. Fig. 2 (right), taken from Ref. [34], illustrates the good quality of the fit. Careful inspection of the figure reveals that at each Q^2 value the fit consists of three lines, whose separation represents the uncertainty.

High- Q^2 continuum: For sufficiently large Q^2 and W^2 one can calculate F_2 and F_L from parton distribution functions (PDFs) using the known perturbative expansion of the DIS coefficient functions. This is more reliable than using a fit to available data (e.g. GD11-P also includes some high- Q^2 data), because the extension to arbitrarily large Q^2 is provided by DGLAP evolution rather than the

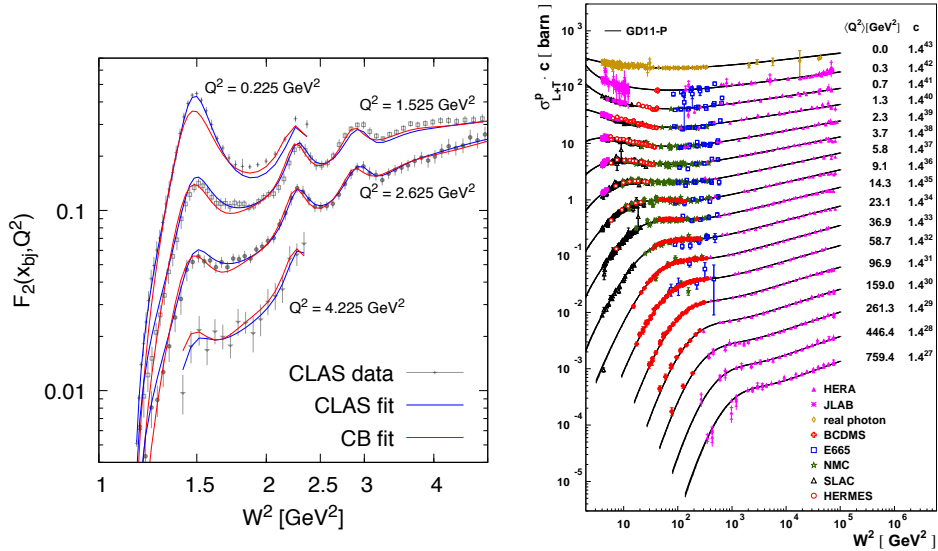


Figure 2: Left: illustration of a subset of the CLAS data [32] in the resonance region, compared to two fits, one from the CLAS paper and the other from Christy and Bosted (CB) [33]. The CLAS dataset covers the range $0.225 \leq Q^2/\text{GeV}^2 \leq 4.725$ in steps of 0.05, with a quality comparable to that shown in the plot across the whole Q^2 range. The errors on the data correspond to the sum in quadrature of statistical and systematic components. The CLAS data is only a small part of the data that is available in the resonance region and used for the fits (see also Fig. 6 of Ref. [32]). Right: illustration of the GD11-P fit from the HERMES collaboration [34] and corresponding data in the continuum region (plot reproduced with kind permission of the HERMES collaboration).

extrapolation provided by some a priori arbitrary parametrisation. Furthermore, in recent years there has been extensive progress in the extraction of PDFs from DIS and collider data, including detailed and well-tested uncertainty estimates.

Our default domain for using a PDF-based evaluation of the structure functions will be $Q^2 > Q_{\text{PDF}}^2 = 9 \text{ GeV}^2$ and $W^2 > 4 \text{ GeV}^2$. In the rest of the kinematic plane we will use the resonance and low Q^2 continuum fits. The breakup of the $x_{\text{bj}}-Q^2$ plane is summarised in Fig. 3. The colour-coding provides a visualisation of the size of the integrand in the sum of Eqs. (3.2, 3.3).

5 Numerical Results and Uncertainties

The photon PDF computed using the method of this paper is given in the left-hand panel of Fig. 4 for $\mu = 100 \text{ GeV}$. It is rescaled by a factor $10^3 x^{0.4}/(1-x)^{4.5}$ to facilitate the simultaneous study of different x regions. The plot includes a

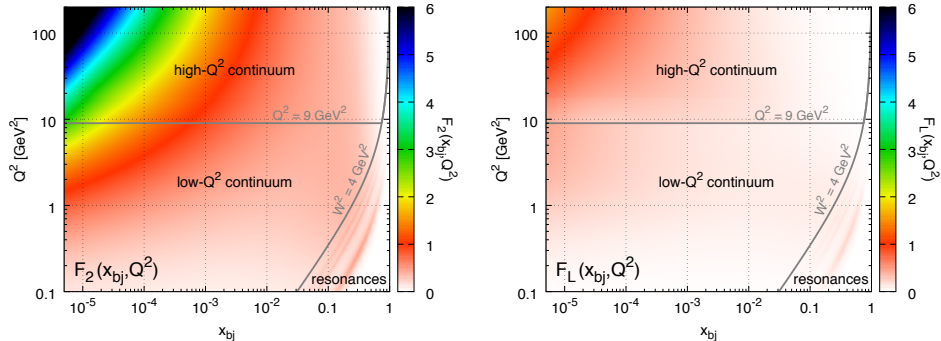


Figure 3: Values of the structure functions F_2 (left) and F_L (right) as a function of x_{bj} and Q^2 , using a PDF4LHC15_nnlo_100-based NNLO ZM-VFNS prescription for $Q^2 > 9 \text{ GeV}^2$ and $W^2 > 4 \text{ GeV}^2$, and the CLAS+GD11-P combination elsewhere.

breakup into the different contributions discussed in Sec. 4. There is a sizeable elastic contribution, with an important magnetic component at large values of x . The resonance and continuum regions are also quantitatively relevant. The white line represents contributions arising from the $Q^2 < 1$ region of all the structure functions, including the full elastic contribution, and this serves to illustrate the importance of a proper inclusion of the low Q^2 region, given the accuracy we aim for. The PDF contribution, in the physical factorisation scheme, is from the bottom of the grey region to the blue dashed curve. The $\overline{\text{MS}}$ -conversion term, Eqs. (3.3), is negative and corresponds to the difference between the blue dashed curve (PF result) and the top edge of the grey region (final full result in the $\overline{\text{MS}}$ scheme).

The right-hand plot of Fig. 4 illustrates how the components evolve when increasing the factorisation scale μ . The main change is associated with the $\log Q^2$ growth of the “PDF” contribution and is most important at small x values, a consequence of the fact that the quarks distributions themselves increase rapidly with Q^2 at small x . The elastic, resonance and (low- Q^2) continuum contributions to the photon PDF all depend slowly on μ via the overall $1/\alpha(\mu^2)$ factor in Eq. (3.2). These components, though formally NLO, remain a significant fraction of the overall photon PDF, even at this large value of μ .

The right panel in Fig. 4 also shows the impact of scale variation on the contributions at $\mu = 500 \text{ GeV}$. The blue dashed curves are for $\mu_M = \mu/2$ and $\mu_M = 2\mu$.⁷ The total $\overline{\text{MS}}$ photon PDF (the top edge of the grey band) uses our central choice of $\mu_M = \mu$. The impact of a change of μ_M on the total photon PDF would be barely visible in the plot, because the substantial scale dependence of the PF result is largely cancelled by that of the $\overline{\text{MS}}$ -conversion term. Previous photon PDFs were at best accurate to leading order, and hence had much larger

⁷The scale μ_M is used instead of μ to split the photon PDF into physical factorization and $\overline{\text{MS}}$ conversion terms. See [27] for details.

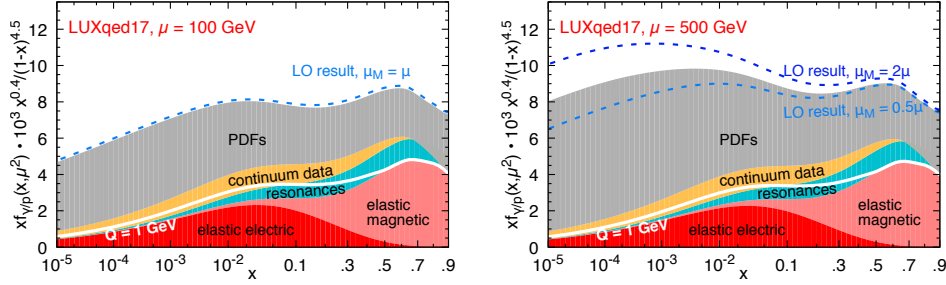


Figure 4: The left panel shows the contributions to the photon PDF at $\mu = 100$ GeV, multiplied by $10^3 x^{0.4}/(1-x)^{4.5}$, with a breakdown into the various components discussed in the text. The white line is the sum of the inelastic contribution from $Q^2 \leq 1$ (GeV) 2 in Eq. (3.2) and the full elastic contribution. The full physical factorisation result of Eq. (3.2), which is equivalent to a LO result, is given by the dashed blue line. The right panel shows the same plot for $\mu = 500$ GeV, with the scale μ_M for the LO results set to $\mu/2$ or 2μ . The total PDF (edge of grey region) is shown for $\mu_M = \mu$. The $\overline{\text{MS}}$ -conversion term (difference between grey region and dashed blue curve) has a significant impact with scale choices other than $\mu_M = \mu$.

scale uncertainties than our determination, which we dubbed “LUXqed”.

The final uncertainty on our PDF distribution is taken to be the sum in quadrature of many individual uncertainty sources, because they are uncorrelated. The individual contributions are discussed in detail in [27]. The various uncertainties with labels as in Fig. 5 are:

- (EFIT) The uncertainty on the elastic contribution that comes from the uncertainty on the A1 world polarised form factor fits. This band is asymmetric and we symmetrise it using the largest deviation to obtain a (more conservative) symmetric band.
- (EUN) The uncertainty that comes from replacing the A1 world polarised fit (which includes a two-photon-exchange correction) with just the world unpolarised data (which does not). This provides a one-sided uncertainty, which we again symmetrise.
- (RES) We replace the CLAS resonance-region fit with the Christy-Bosted fit. This replacement gives a one-sided uncertainty, which we once again symmetrise.
- (R) A modification of $R_{L/T}$ (used to parameterize F_L) by $\pm 50\%$ around its central value.
- (M) A modification of the Q_{PDF}^2 scale which governs the transition from the GD11-P structure function fit to a PDF-based evaluation. The default choice of $Q_{\text{PDF}}^2 = 9$ GeV 2 is reduced to 5 GeV 2 and since this is a one-sided uncertainty, the resulting effect is symmetrised.
- (PDF) The input PDF uncertainties for $Q^2 > Q_{\text{PDF}}^2$ according to the default prescription for the PDF (PDF4LHC15_nnlo_100 [36]).
- (T) A twist-four modification of F_L . This is a one-sided modification that is then

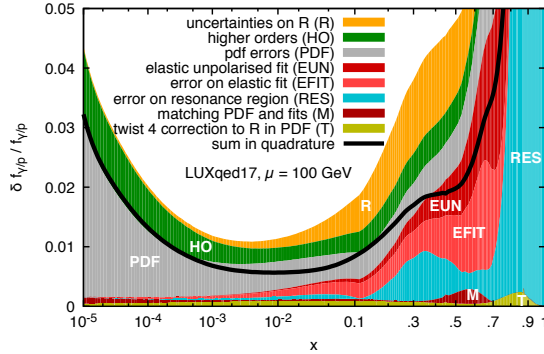


Figure 5: Breakdown of uncertainties on the photon distribution. The uncertainties are shown stacked linearly, while the sum in quadrature, i.e. our final uncertainty, is represented by the thick black line. See the text for a detailed description of the various contributions.

symmetrised.

- (HO) An estimate of missing higher-order effects obtained by taking the largest deviation of any of the NNLO results relative to the NLO result. The resulting uncertainty is symmetrised.

The impact of the different sources of uncertainty is shown in Fig. 5, and our final uncertainty, shown by the black line, is given by adding the contributions in quadrature.⁸ The overall uncertainty is less than 2% for $10^{-4} < x < 0.1$. For small values of x , the uncertainty is dominated by the uncertainties in the parton distributions of quarks (and gluons), which enter the high- Q^2 part of the photon PDF integral. As $x \rightarrow 1$, the uncertainties are dominated by the low- Q^2 part of the photon PDF integral from elastic form factors, the resonance contribution, and σ_L . This is a reflection of the fact that non-perturbative effects (such as higher twist corrections) grow like $\Lambda_{\text{QCD}}^2/[Q^2(1-x)]$ as $x \rightarrow 1$, and that, for x close to 1, quark PDFs fall off rapidly as Q^2 increases, so the low- Q^2 region contributes significantly to f_γ as $x \rightarrow 1$.

The resulting PDF was released in LHAPDF format [37] as sets that augment the PDF4LHC15 set, notably as `LUXqed17_plus_PDF4LHC15_nnlo_100` and `LUXqed17_plus_PDF4LHC15_nnlo_30`. Note that this also involved adjustments of the distributions of other flavours so as to ensure a consistent momentum sum, as well as the correct QED evolution of the quark flavours.

⁸There are correlations between high and low Q^2 that have not been included in our analysis. For example, low Q^2 values for $F_2(x, Q^2)$ are correlated with quark and gluon PDFs at high Q^2 , via DGLAP evolution of F_2 .

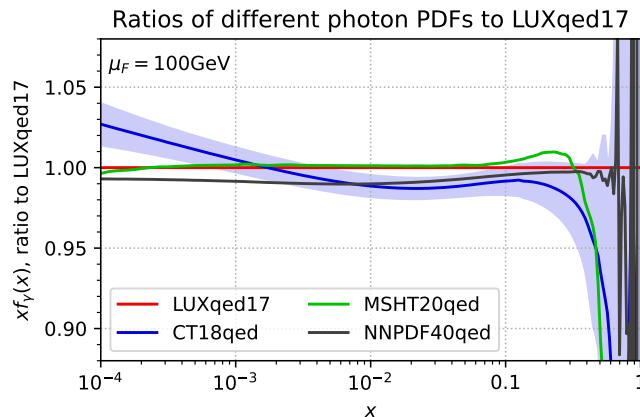


Figure 6: Comparison of recent determinations of photon distributions based on the LUXqed method, taking the latest NNLO set from each group.

6 Recent developments, applications and spin-offs

6.1 Global fits including the photon PDF

Since the original proposal, all major PDF fitting collaborations have adopted the LUXqed approach for the determination of the photon. In particular the NNPDF collaboration has included it as part of the NNPDF3.1luxQED [38] set as well as the more recent NNPDF4.0QED [39] and the NNPDF40MC QED sets for Monte Carlo event simulation [40]. The MSHT group adapted the approach to develop the Ad Lucem framework [41], yielding MSHT20qed [42] (including separation into elastic and inelastic PDFs) and incorporating it also into their recent approximate N3LO [43] fits MSHT20qed_an3lo [44]. The CTEQ-TEA collaboration developed the CT18qed set [45], which apply Eqs. (3.1)–(3.3) across scales or at an initial scale followed by QED evolution and they have also used the same approach to determine the photon content of the neutron [46]. One advantage of carrying out a full PDF fit at the same time as the photon-distribution determination is that it makes it possible to consistently take into account the interplay between the photon and other partons in the PDF. Fig. 6 compares the photon distributions from different groups, illustrating the generally good agreement between them. The small residual differences that are visible may have several origins, for example different high-scale quark distributions, and the choice of the initial scale where Eq. (3.1) is used to evaluate the photon PDF (LUXqed17 and NNPDF40qed use a scale of 100 GeV to minimise higher-twist effects in the photon, whereas CT18qed and MSHT20qed use scales respectively of 1.3 and 1 GeV respectively).

6.2 Lepton PDFs

Virtual leptons in the proton can only arise through the production of an intermediate photon. It then turns out that the lepton PDFs can be computed from the hadronic structure functions and form factors, using the same experimental input used in the case of the photon. The computation (which is considerably more complex) was carried out in ref. [47], and it led to the generation of proton PDFs including photons and leptons. It was pointed out there that lepton scattering processes were calculable in terms of lepton PDFs, and that in some cases they could be detectable as back to back pairs of leptons with different flavours and/or with the same electric charge. Furthermore, some BSM processes became calculable. In particular, resonant lepto-quark production was a particularly interesting one, and was studied in [48]. The calculation of lepton scattering processes and of lepto-quark production were extended to next-to-leading order in [49–52].

6.3 Experimental studies using LUX photon or lepton PDFs

The LUX photon PDF has been instrumental in precise predictions of photon-initiated processes, as well as in the calculation of electroweak corrections to hadronic cross sections at the LHC. This has significantly improved the accuracy of theoretical predictions and enhanced the reliability of comparisons with experimental data. Accordingly, the LUX determination of the photon PDF has been widely utilized in a variety of Standard Model measurements, which either involve the photon PDF directly at leading order or indirectly through higher-order processes, such as those involving electroweak (EW) corrections. For instance it has been used in

- the measurements of $t\bar{t}$ differential cross sections using events containing two leptons [53],
- the measurement of differential cross sections for the production of top quark pairs and of additional jets in lepton+jets [54],
- the measurement of top differential kinematics, including EW corrections [55],
- the measurement of the differential Drell-Yan cross section [56],
- the exclusive $\gamma\gamma \rightarrow \mu^+\mu^-$ production [57],
- the measurement of the top charged asymmetry including EW effects [58],
- the measurement of the mass dependence of the transverse momentum of lepton pairs in Drell-Yan production [59],
- the measurement of the Drell-Yan forward-backward asymmetry at high dilepton masses in proton-proton [60],
- the measurement of the Higgs boson width and evidence of its off-shell contributions to ZZ production [61].

Furthermore, the LUX determination of the photon and lepton PDFs has played a critical role in a wide array of searches for new physics at the LHC. These PDFs are essential for accurately modeling photon- and lepton-initiated processes, which are often key components in the search for signals beyond the Standard Model. By providing more precise predictions for the SM backgrounds in these channels, the LUX PDFs have improved the sensitivity of these searches, allowing

for tighter constraints on new physics scenarios. Some specific LHC searches where the LUX PDFs have been utilized include:

- the search for heavy long-lived multi-charged particles [62],
- the search for magnetic monopoles and stable particles with high electric charges [63],
- the search for heavy neutral Higgs bosons decaying into a top quark pair [64],
- the search for vector-boson resonances decaying into a top quark and a bottom quark [65],
- the search for heavy neutral leptons in final states with electrons, muons, and hadronically decaying tau leptons [66],
- the search for t -channel scalar and vector leptoquark exchange in the high mass dimuon and dielectron spectrum [67],
- the search for new physics in final states with a single photon and missing transverse momentum [68],
- the search for Scalar Leptoquarks Produced via τ -Lepton–Quark Scattering [69],
- the search for new physics in the lepton plus missing transverse momentum final state [70],
- the search for resonant and non-resonant new phenomena in high-mass dilepton final states [71],
- the search for contact interactions and large extra dimensions in the dilepton mass spectra [72],
- the search for heavy Majorana neutrinos in same-sign dilepton channels [73],
- the search for a new scalar resonance decaying to a pair of Z bosons [74],
- the search for high-mass resonances in dilepton final states [75],
- the search for heavy neutral leptons in events with three charged leptons [76].

7 Conclusions

The photon PDF is important for both precision physics and LHC searches, as the experiments are now sensitive to electromagnetic (and electroweak) radiative corrections. The photon PDF is a non-perturbative quantity. Our method allows us to compute it by dividing it into (a) a non-perturbative physical factorisation contribution which is determined exactly in terms of measured non-perturbative quantities, the deep-inelastic structure functions and electric and magnetic proton form factors (b) The $\overline{\text{MS}}$ conversion term which can be computed relatively simply in perturbation theory.

Our method reduced the error on the photon PDF by a factor of forty over previous results, to $\lesssim 2\%$. The computation is a (unique?) example where great improvement in precision for a QCD quantity was achieved without very involved calculations. It also provides a nice example where experiments over a wide energy range, from low-energy nuclear form factor and ep scattering measurements to higher energy deep-inelastic scattering combine to give a result that is important for high energy physics and BSM searches. It opens up many new possibilities to use data from the Large Hadron Collider.

Acknowledgements

The work done in Refs. [1, 27] was supported in part by ERC Consolidator Grant HICCUP (No. 614577), ERC Advanced Grant Higgs@LHC (No. 321133), a Simons Foundation grant (#340281 to AM), by DOE grant DE-SC0009919, and NSF grant NSF PHY11-25915. AM and PN acknowledge CERN-TH for hospitality, GPS and GZ thank KITP, and AM, GPS and GZ thank MIAPP for hospitality while parts of the work were being completed. We thank ICBS for having selected our paper [1] for a FSA award in theoretical physics.

References

- [1] A. Manohar, P. Nason, G. P. Salam and G. Zanderighi, *How bright is the proton? A precise determination of the photon parton distribution function*, Phys. Rev. Lett. **117** (2016) 242002 [1607.04266].
- [2] E. Fermi, *On the Theory of the impact between atoms and electrically charged particles*, Z. Phys. **29** (1924) 315.
- [3] C. F. von Weizsacker, *Radiation emitted in collisions of very fast electrons*, Z. Phys. **88** (1934) 612.
- [4] E. J. Williams, *Nature of the high-energy particles of penetrating radiation and status of ionization and radiation formulae*, Phys. Rev. **45** (1934) 729.
- [5] M. Ciccolini, A. Denner and S. Dittmaier, *Electroweak and QCD corrections to Higgs production via vector-boson fusion at the LHC*, Phys. Rev. **D77** (2008) 013002 [0710.4749].
- [6] A. Denner, S. Dittmaier, S. Kallweit and A. Muck, *Electroweak corrections to Higgs-strahlung off W/Z bosons at the Tevatron and the LHC with HAWK*, JHEP **03** (2012) 075 [1112.5142].
- [7] LHC HIGGS CROSS SECTION WORKING GROUP collaboration, *Handbook of LHC Higgs Cross Sections: 4. Deciphering the Nature of the Higgs Sector*, 1610.07922.
- [8] ATLAS collaboration, *Measurement of the transverse momentum and ϕ_n^* distributions of Drell–Yan lepton pairs in proton–proton collisions at $\sqrt{s} = 8$ TeV with the ATLAS detector*, Eur. Phys. J. **C76** (2016) 291 [1512.02192].
- [9] ATLAS collaboration, *Measurement of the double-differential high-mass Drell–Yan cross section in pp collisions at $\sqrt{s} = 8$ TeV with the ATLAS detector*, 1606.01736.
- [10] E. Accomando, J. Fiaschi, F. Hautmann, S. Moretti and C. H. Shepherd-Themistocleous, *Photon-initiated production of a di-lepton final state at the LHC: cross section versus forward-backward asymmetry studies*, 1606.06646.
- [11] S. Alioli et al., *Precision Studies of Observables in $pp \rightarrow W \rightarrow \ell\nu$ and $pp \rightarrow \gamma, Z \rightarrow \ell^+\ell^-$ processes at the LHC*, 1606.02330.
- [12] D. Bourilkov, *Photon-induced Background for Dilepton Searches and Measurements in pp Collisions at 13 TeV*, 1606.00523.
- [13] D. Pagani, I. Tsinikos and M. Zaro, *The impact of the photon PDF and electroweak corrections on $t\bar{t}$ distributions*, 1606.01915.

- [14] M. Luszczak, A. Szczurek and C. Royon, *W^+W^- pair production in proton-proton collisions: small missing terms*, JHEP **02** (2015) 098 [1409.1803].
- [15] A. Denner, S. Dittmaier, M. Hecht and C. Pasold, *NLO QCD and electroweak corrections to $Z + \gamma$ production with leptonic Z-boson decays*, JHEP **02** (2016) 057 [1510.08742].
- [16] M. Ababekri, S. Dulat, J. Isaacson, C. Schmidt and C. P. Yuan, *Implication of CMS data on photon PDFs*, 1603.04874.
- [17] B. Biedermann, A. Denner, S. Dittmaier, L. Hofer and B. Jäger, *Electroweak corrections to $pp \rightarrow \mu^+\mu^-e^+e^- + X$ at the LHC: a Higgs background study*, Phys. Rev. Lett. **116** (2016) 161803 [1601.07787].
- [18] B. Biedermann, M. Billoni, A. Denner, S. Dittmaier, L. Hofer, B. Jäger et al., *Next-to-leading-order electroweak corrections to $pp \rightarrow W^+W^- \rightarrow 4$ leptons at the LHC*, JHEP **06** (2016) 065 [1605.03419].
- [19] W. Yong, Z. Ren-You, M. Wen-Gan, L. Xiao-Zhou and G. Lei, *NLO QCD and electroweak corrections to $ZZ + \text{jet}$ production with Z-boson leptonic decays at LHC*, 1604.04080.
- [20] S. Kallweit, J. M. Lindert, S. Pozzorini and M. Schonherr, *NLO QCD+EW predictions for $2\ell 2\nu$ diboson signatures at the LHC*, 1705.00598.
- [21] A. D. Martin, R. G. Roberts, W. J. Stirling and R. S. Thorne, *Parton distributions incorporating QED contributions*, Eur. Phys. J. **C39** (2005) 155 [hep-ph/0411040].
- [22] NNPDF collaboration, *Parton distributions with QED corrections*, Nucl. Phys. **B877** (2013) 290 [1308.0598].
- [23] C. Schmidt, J. Pumplin, D. Stump and C. P. Yuan, *CT14QED parton distribution functions from isolated photon production in deep inelastic scattering*, Phys. Rev. **D93** (2016) 114015 [1509.02905].
- [24] L. A. Harland-Lang, V. A. Khoze and M. G. Ryskin, *Photon-initiated processes at high mass*, Phys. Rev. **D94** (2016) 074008 [1607.04635].
- [25] *Search for resonances decaying to photon pairs in 3.2 fb^{-1} of pp collisions at $\sqrt{s} = 13 \text{ TeV}$ with the ATLAS detector*, Tech. Rep. ATLAS-CONF-2015-081, CERN, Geneva, Dec, 2015.
- [26] CMS COLLABORATION collaboration, *Search for new physics in high mass diphoton events in proton-proton collisions at $\sqrt{s} = 13 \text{ TeV}$* , Tech. Rep. CMS-PAS-EXO-15-004, CERN, Geneva, 2015.
- [27] A. V. Manohar, P. Nason, G. P. Salam and G. Zanderighi, *The Photon Content of the Proton*, JHEP **12** (2017) 046 [1708.01256].
- [28] M. Drees and D. Zeppenfeld, *Production of Supersymmetric Particles in Elastic ep Collisions*, Phys. Rev. **D39** (1989) 2536.
- [29] H. Anlauf, H. D. Dahmen, P. Manakos, T. Mannel and T. Ohl, *KRONOS: A Monte Carlo event generator for higher order electromagnetic radiative corrections to deep inelastic scattering at HERA*, Comput. Phys. Commun. **70** (1992) 97.
- [30] A. Mukherjee and C. Pisano, *Manifestly covariant analysis of the QED Compton process in $ep \rightarrow e\gamma p$ and $ep \rightarrow e\gamma X$* , Eur. Phys. J. **C30** (2003) 477 [hep-ph/0306275].

- [31] A1 collaboration, *Electric and magnetic form factors of the proton*, Phys. Rev. **C90** (2014) 015206 [1307.6227].
- [32] CLAS collaboration, *A Kinematically complete measurement of the proton structure function $F(2)$ in the resonance region and evaluation of its moments*, Phys. Rev. **D67** (2003) 092001 [hep-ph/0301204].
- [33] M. E. Christy and P. E. Bosted, *Empirical fit to precision inclusive electron-proton cross- sections in the resonance region*, Phys. Rev. **C81** (2010) 055213 [0712.3731].
- [34] HERMES collaboration, *Inclusive Measurements of Inelastic Electron and Positron Scattering from Unpolarized Hydrogen and Deuterium Targets*, JHEP **05** (2011) 126 [1103.5704].
- [35] H. Abramowicz, E. M. Levin, A. Levy and U. Maor, *A Parametrization of $\sigma_T(\gamma^*p)$ above the resonance region $Q^2 \geq 0$* , Phys. Lett. **B269** (1991) 465.
- [36] J. Butterworth et al., *PDF4LHC recommendations for LHC Run II*, J. Phys. **G43** (2016) 023001 [1510.03865].
- [37] A. Buckley, J. Ferrando, S. Lloyd, K. Nordström, B. Page, M. Rüfenacht et al., *LHAPDF6: parton density access in the LHC precision era*, Eur. Phys. J. **C75** (2015) 132 [1412.7420].
- [38] NNPDF collaboration, *Illuminating the photon content of the proton within a global PDF analysis*, SciPost Phys. **5** (2018) 008 [1712.07053].
- [39] NNPDF collaboration, *Photons in the proton: implications for the LHC*, Eur. Phys. J. C **84** (2024) 540 [2401.08749].
- [40] J. Cruz-Martinez, S. Forte, N. Laurenti, T. R. Rabemananjara and J. Rojo, *LO, NLO, and NNLO Parton Distributions for LHC Event Generators*, 2406.12961.
- [41] L. A. Harland-Lang, A. D. Martin, R. Nathvani and R. S. Thorne, *Ad Lucem: QED Parton Distribution Functions in the MMHT Framework*, Eur. Phys. J. C **79** (2019) 811 [1907.02750].
- [42] T. Cridge, L. A. Harland-Lang, A. D. Martin and R. S. Thorne, *QED parton distribution functions in the MSHT20 fit*, Eur. Phys. J. C **82** (2022) 90 [2111.05357].
- [43] J. McGowan, T. Cridge, L. A. Harland-Lang and R. S. Thorne, *Approximate N^3LO parton distribution functions with theoretical uncertainties: MSHT20a N^3LO PDFs*, Eur. Phys. J. C **83** (2023) 185 [2207.04739], [Erratum: Eur.Phys.J.C 83, 302 (2023)].
- [44] T. Cridge, L. A. Harland-Lang and R. S. Thorne, *Combining QED and Approximate N^3LO QCD Corrections in a Global PDF Fit: MSHT20qed.an3lo PDFs*, SciPost Phys. **17** (2024) 026 [2312.07665].
- [45] CTEQ-TEA collaboration, *Photon PDF within the CT18 global analysis*, Phys. Rev. D **105** (2022) 054006 [2106.10299].
- [46] CTEQ-TEA collaboration, *The photon content of the neutron*, JHEP **04** (2024) 022 [2305.10497].
- [47] L. Buonocore, P. Nason, F. Tramontano and G. Zanderighi, *Leptons in the proton*, JHEP **08** (2020) 019 [2005.06477].
- [48] L. Buonocore, U. Haisch, P. Nason, F. Tramontano and G. Zanderighi, *Lepton-Quark Collisions at the Large Hadron Collider*, Phys. Rev. Lett. **125**

- (2020) 231804 [2005.06475].
- [49] L. Buonocore, P. Nason, F. Tramontano and G. Zanderighi, *Photon and leptons induced processes at the LHC*, JHEP **12** (2021) 073 [2109.10924].
 - [50] A. Greljo and N. Selimovic, *Lepton-Quark Fusion at Hadron Colliders, precisely*, JHEP **03** (2021) 279 [2012.02092].
 - [51] L. Buonocore, A. Greljo, P. Krack, P. Nason, N. Selimovic, F. Tramontano et al., *Resonant leptoquark at NLO with POWHEG*, JHEP **11** (2022) 129 [2209.02599].
 - [52] U. Haisch and G. Polesello, *Resonant third-generation leptoquark signatures at the Large Hadron Collider*, JHEP **05** (2021) 057 [2012.11474].
 - [53] CMS collaboration, *Measurements of $t\bar{t}$ differential cross sections in proton-proton collisions at $\sqrt{s} = 13$ TeV using events containing two leptons*, JHEP **02** (2019) 149 [1811.06625].
 - [54] CMS collaboration, *Measurement of differential cross sections for the production of top quark pairs and of additional jets in lepton+jets events from pp collisions at $\sqrt{s} = 13$ TeV*, Phys. Rev. D **97** (2018) 112003 [1803.08856].
 - [55] ATLAS collaboration, *Measurements of top-quark pair differential and double-differential cross-sections in the ℓ +jets channel with pp collisions at $\sqrt{s} = 13$ TeV using the ATLAS detector*, Eur. Phys. J. C **79** (2019) 1028 [1908.07305], [Erratum: Eur.Phys.J.C 80, 1092 (2020)].
 - [56] CMS collaboration, *Measurement of the differential Drell-Yan cross section in proton-proton collisions at $\sqrt{s} = 13$ TeV*, JHEP **12** (2019) 059 [1812.10529].
 - [57] ATLAS collaboration, *Measurement of the exclusive $\gamma\gamma \rightarrow \mu^+\mu^-$ process in proton-proton collisions at $\sqrt{s} = 13$ TeV with the ATLAS detector*, Phys. Lett. B **777** (2018) 303 [1708.04053].
 - [58] ATLAS collaboration, *Evidence for the charge asymmetry in $pp \rightarrow t\bar{t}$ production at $\sqrt{s} = 13$ TeV with the ATLAS detector*, JHEP **08** (2023) 077 [2208.12095].
 - [59] CMS collaboration, *Measurement of the mass dependence of the transverse momentum of lepton pairs in Drell-Yan production in proton-proton collisions at $\sqrt{s} = 13$ TeV*, Eur. Phys. J. C **83** (2023) 628 [2205.04897].
 - [60] CMS collaboration, *Measurement of the Drell-Yan forward-backward asymmetry at high dilepton masses in proton-proton collisions at $\sqrt{s} = 13$ TeV*, JHEP **2022** (2022) 063 [2202.12327].
 - [61] CMS collaboration, *Measurement of the Higgs boson width and evidence of its off-shell contributions to ZZ production*, Nature Phys. **18** (2022) 1329 [2202.06923].
 - [62] ATLAS collaboration, *Search for heavy long-lived multi-charged particles in the full LHC Run 2 pp collision data at $s=13$ TeV using the ATLAS detector*, Phys. Lett. B **847** (2023) 138316 [2303.13613].
 - [63] ATLAS collaboration, *Search for magnetic monopoles and stable particles with high electric charges in $\sqrt{s} = 13$ TeV pp collisions with the ATLAS detector*, JHEP **11** (2023) 112 [2308.04835].
 - [64] ATLAS collaboration, *Search for heavy neutral Higgs bosons decaying into a*

- top quark pair in 140 fb^{-1} of proton-proton collision data at $\sqrt{s} = 13 \text{ TeV}$ with the ATLAS detector*, 2404.18986.
- [65] ATLAS collaboration, *Search for vector-boson resonances decaying into a top quark and a bottom quark using pp collisions at $\sqrt{s} = 13 \text{ TeV}$ with the ATLAS detector*, JHEP **12** (2023) 073 [2308.08521].
- [66] CMS collaboration, *Search for heavy neutral leptons in final states with electrons, muons, and hadronically decaying tau leptons in proton-proton collisions at $\sqrt{s} = 13 \text{ TeV}$* , JHEP **06** (2024) 123 [2403.00100].
- [67] CMS collaboration, *Search for t-channel scalar and vector leptoquark exchange in the high mass dimuon and dielectron spectrum in proton-proton collisions at $\sqrt{s} = 13 \text{ TeV}$* , .
- [68] CMS collaboration, *Search for new physics in final states with a single photon and missing transverse momentum in proton-proton collisions at $\sqrt{s} = 13 \text{ TeV}$* , JHEP **02** (2019) 074 [1810.00196].
- [69] CMS collaboration, *Search for Scalar Leptoquarks Produced via τ -Lepton-Quark Scattering in pp Collisions at $s=13 \text{ TeV}$* , Phys. Rev. Lett. **132** (2024) 061801 [2308.06143].
- [70] CMS collaboration, *Search for new physics in the lepton plus missing transverse momentum final state in proton-proton collisions at $\sqrt{s} = 13 \text{ TeV}$* , JHEP **07** (2022) 067 [2202.06075].
- [71] CMS collaboration, *Search for resonant and nonresonant new phenomena in high-mass dilepton final states at $\sqrt{s} = 13 \text{ TeV}$* , JHEP **07** (2021) 208 [2103.02708].
- [72] CMS collaboration, *Search for contact interactions and large extra dimensions in the dilepton mass spectra from proton-proton collisions at $\sqrt{s} = 13 \text{ TeV}$* , JHEP **04** (2019) 114 [1812.10443].
- [73] CMS collaboration, *Search for heavy Majorana neutrinos in same-sign dilepton channels in proton-proton collisions at $\sqrt{s} = 13 \text{ TeV}$* , JHEP **01** (2019) 122 [1806.10905].
- [74] CMS collaboration, *Search for a new scalar resonance decaying to a pair of Z bosons in proton-proton collisions at $\sqrt{s} = 13 \text{ TeV}$* , JHEP **06** (2018) 127 [1804.01939], [Erratum: JHEP 03, 128 (2019)].
- [75] CMS collaboration, *Search for high-mass resonances in dilepton final states in proton-proton collisions at $\sqrt{s} = 13 \text{ TeV}$* , JHEP **06** (2018) 120 [1803.06292].
- [76] CMS collaboration, *Search for heavy neutral leptons in events with three charged leptons in proton-proton collisions at $\sqrt{s} = 13 \text{ TeV}$* , Phys. Rev. Lett. **120** (2018) 221801 [1802.02965].

DEPARTMENT OF PHYSICS, UNIVERSITY OF CALIFORNIA AT SAN DIEGO,
9500 GILMAN DRIVE, LA JOLLA, CA 92093-0319, USA.

E-mail address: amanohar@ucsd.edu

UNIVERSITÀ DI MILANO-BICOCCA AND INFN, SEZIONE DI MILANO-BICOCCA,
PIAZZA DELLA SCIENZA 3, 20126 MILANO, ITALY.

E-mail address: `paolo.nason@mib.infn.it`

RUDOLF PEIERLS CENTRE FOR THEORETICAL PHYSICS,
CLARENDON LABORATORY, PARKS ROAD, OXFORD OX1 3PU, UK
AND ALL SOULS COLLEGE, OXFORD OX1 4AL, UK

E-mail address: `gavin.salam@physics.ox.ac.uk`

MAX-PLANCK-INSTITUT FÜR PHYSIK, BOLTZMANNSTRASSE 8, AND
TECHNISCHE UNIVERSITÄT MÜNCHEN, JAMES-FRANCK-STRASSE 1,
85748 GARCHING, GERMANY. *E-mail address:* `zanderi@mpp.mpg.de`

